Construction and Building Materials xxx (xxxx) xxx

Contents lists available at ScienceDirect

Construction and Building Materials

journal homepage: www.elsevier.com/locate/conbuildmat

Optimization of mechanical strength of biocemented Martian regolith simulant soil columns

Jason Gleaton [a], Zhengshou Lai [b,c], Rui Xiao [a], Ke Zhang [d,1], Qiushi Chen [e], Yi Zheng [d,*]

[a] Department of Environmental Engineering and Earth Sciences, Clemson University, 342 Computer Court, Anderson, SC 29625, USA
[b] School of Intelligent Systems Engineering, Sun Yat-sen University, Shenzhen 518107, China
[c] Department of Civil and Environmental Engineering, The Hong Kong University of Science and Technology, Hong Kong, China
[d] Department of Grain Science and Industry, Kansas State University, 101C BIVAP, 1980 Kimball Avenue, Manhattan, KS 66506, USA
[e] Glenn Department of Civil Engineering, Clemson University, 320 Lowry Hall, Clemson, SC 29634, USA

ARTICLE INFO

Keywords:
Biocementation
Biogrout
Martian regolith simulant
Thraustochytrium striatum
Unconfined compressive strength
Response surface methodology

ABSTRACT

Biocemented Martian regolith simulant (MRS) columns were developed using a microalga, *Thraustochytrium striatum*. Response surface methodology was used to maximize the unconfined compressive strength (UCS) of biocemented MRS columns towards regolith particle size, cell biomass loading, and nutrient ($CaCl_2$/urea) loading. Overall, the UCS increased with the increase of cell biomass loading while the MRS of medium particle size achieved the highest UCS. But the nutrient loading didn't show a consistent effect. The maximum UCS reached 603.83 kPa with 0.25 ~ 0.425 mm particle size, 3.8 g/100 mL cell biomass loading, 5.83 g/100 mL $CaCl_2$ loading, and 14.18 g/100 mL urea loading.

1. Introduction

Biocementation takes advantage of microbially induced carbonate precipitation (MICP) mechanism to create the deposition of calcium carbonate ($CaCO_3$) as a binding agent [1,2]. During MICP, biocement is generated in the spaces between particles of granular materials (e.g., sand) when a stream of liquid containing MICP-enabling microorganism, urea (as a substrate), and calcium ion (e.g., $CaCl_2$) [3]. Various types of microorganisms can cause MICP, such as photosynthetic organisms, sulfate reducing bacteria, and organisms that utilize nitrogen cycle [4,5]. The most studied type for biocementation is urease-producing organisms (e.g., *Sporosarcina pasteurii*) [6–8]. These organisms produce urease that hydrolyzes urea and generates CO_3^{2-} at basic pH so that $CaCO_3$ crystals are formed as biocement in the presence of calcium ion. The biocement bonds the sand grains together to create a solidified sandstone. The binding of grains and $CaCO_3$ crystals could result from the SiO_2 transformation on the sand surface to form a glue layer of ammonium silicate water glass, $(NH_4)_2Si(OH)_4$ which binds $CaCO_3$ crystals [9]. This gel on the sand surface is hardened after the biocemented sample is dried, thus the mechanical strength of the biocemented sand increased significantly.

Compared with conventional cement, the advantages of cementing loose sand with MICP technology include lower permeability coefficient, more environmentally friendly, controllable reaction process, more energy- and cost-efficient, and long transmission distance [10,11]. Therefore, biocementation has received extensive research in repairing damaged concrete structures (e.g., bridge and road surface fissure repair), improving soil stabilization, and replacing conventional cement in construction materials [12–15]. This technology appears to be promising in sustainable structural and geotechnical applications. Encouraged by the success in laboratory research, biocementation has already been used in field applications, such as monumental stone reinforcement, sealing of parking garage crack, and ground improvement [3].

In our previous biocementation study [16], *Thraustochytrium striatum*, a marine microalga, was found effective and efficient in creating MICP for the production of biocemented Martian regolith simulant (MRS) columns, which has the potential as an earth-independent construction material for space applications. However, the effects of several key factors (e.g., MRS particle size, cell biomass loading, and calcium/urea loadings) on the mechanical strength of MRS columns haven't been studied or optimized. All these factors have been identified in previous studies to significantly affect the properties of biocemented soil columns, though the conclusions are different, sometimes even

* Corresponding author.
E-mail address: yzheng@ksu.edu (Y. Zheng).
[1] Present address: Novozymes North America Inc., PO BOX 576, 77 Perrys Chapel Church Road, Franklinton, NC 27525, USA.

https://doi.org/10.1016/j.conbuildmat.2021.125741
Received 3 June 2021; Received in revised form 6 September 2021; Accepted 16 November 2021

contradictory, among various studies. Grain size had a significant effect on the unconfined compressive strength (UCS) of biocemented granular columns. Hoang et al. [17] studied soil stabilization by *S. pasteurii* using coarse- and fine-grained sand and reported that coarse-grained biocemented sand had much higher UCS than fine-grained treated sand even at similar levels of $CaCO_3$ produced during biocementation. They concluded that the $CaCO_3$ content is not the sole factor impacting the strength of biocemented sand. Similarly, Yang et al. [11] and Terzis and Laloui [18] found the UCS of biocemented sand column was improved by increasing the sand particle size, and the increase of particle size led to more uniform spatial distribution of $CaCO_3$ in the biocemented sand column. Compared to the content of $CaCO_3$ precipitate, the particle size of $CaCO_3$ bond lattice, bond-grain contact, and bond particle orientation are more important for the mechanical strength of biocemented sandstones [18]. In contrast, Mahawish et al. [19] showed that mixing fine and coarse grains provided more bridging contacts (connected by $CaCO_3$ precipitate) between coarse grains so that a gap-graded particle size distribution improved the UCS of biocemented coarse grains. They also found that the maximum UCS was not necessarily linked with the maximum $CaCO_3$ precipitation.

In addition to particle size, nutrients such as urea and calcium salt concentrations are also critical for the property of biocemented granular columns. In studying the effects of calcium salt and urea concentrations on the effectiveness of biocementation, De Muynck et al. [20] found that the consolidation and stabilization of ornamental stone was improved with the increase of $CaCl_2$ and urea dosages but was not further improved when Ca^{2+} exceeded a certain level of dosage. It was indicated that the calcite precipitation ratio declined at higher nutrient concentrations due to microbial activity inhibition by high salinity [21,22], while this ratio increased with higher urease activity [17]. Yang et al. [11] and Mortensen et al. [23] also found that low concentration of nutrients led to the increase of $CaCO_3$ precipitate and its spatial distribution uniformity as well as UCS of the sand columns. In investigating the effect of environmental conditions on MICP, Okwadha and Li [24] and Soon et al. [25] revealed that the urea hydrolysis rate, $CaCO_3$ precipitate, and UCS increased with the increase of urea and calcium ion concentrations, while the interactions of urea, calcium ion, and bacterial cells had a significant effect on MICP. Thus, the nutrient concentration should be properly controlled to achieve high urease activity and good biocementation results.

As a biocatalyst of MICP, microbial cell biomass concentration is one of the most important factors influencing the mechanical properties of biocemented sandstones. Cells produce urease and determine ureolysis rate so that high cell concentration increases ureolysis rate and $CaCO_3$ precipitate. To improve the engineering properties of tropical residual soil, Soon et al. [25] studied several experimental conditions of MICP with *Bacillus megaterium* and found that the preferable cell concentration of 10^8 colony forming unit (CFU)/mL achieved comparable shear strength to the treated fine sand. Okwadha and Li [24] revealed that ureolysis rate increased with *S. pasteurii* cell concentration while increasing cell concentration from 10^6 to 10^8 cells/mL increased $CaCO_3$ precipitate by over 30%. However, Yang et al. [11] reported that low *S. pasteurii* cell concentration led to the increase of $CaCO_3$ and UCS. Rowshanbakht et al. [26] also found reducing cell concentration did not affect the mechanical strength of sand specimens, while improving the MICP efficiency, economics, and engineering application feasibility. Thus, the optimum cell concentration varies between specific MICP systems.

Given the impacts of environmental conditions on MICP, the specific objective of this investigation was to optimize biocementation of MRS with *T. striatum* under different conditions regarding three factors, including 1) regolith particle sizes, 2) cell biomass loadings, and 3) $CaCl_2$ and urea loadings to maximize UCS of biocemented MRS columns. A full factorial design with three-factor by three-level was used for experiment arrangement, and the $CaCO_3$ precipitate and UCS were measured for each MRS column. UCS data were analyzed using the response surface methodology (RSM) to develop a statistical regression model, identify the effect of each factor on UCS, and determine an optimum combination of three factors to achieve the maximum UCS of MRS columns with *T. striatum*.

2. Materials and methods

2.1. Preparation of biocementation culture and Martian regolith simulant

The biocementation microorganism used in this study was *T. striatum* ATCC 24,473 which was bought from the American Type Culture Collection (ATCC). The protocol provided by the ATCC was followed to prepare stock culture. Briefly, the stock culture was grown and stored on agar plates at room temperature. The agar plate medium contained the following ingredients (per liter): 30.0 g of glucose, 6.0 g of yeast extract, 6.0 g of peptone, and 10.0 g of agar in artificial seawater (ASW). The ASW contained (per liter): 30.0 g of NaCl, 0.7 of KCl, 10.8 g of $MgCl_2{\cdot}6H_2O$, 5.4 g of $MgSO_4{\cdot}7H_2O$, and 1.0 g of $CaCl_2{\cdot}2H_2O$. The pH of the medium was adjusted to 7.0 using 1 M NaOH and HCl, and the medium was autoclaved at 121 °C for 15 min for sterilization. To prepare the seed culture, a single colony was aseptically transferred from the agar plate to 50 mL sterilized liquid medium in 250-mL flasks, which were incubated at room temperature with a shaking speed of 140 rpm until the cell growth reached the mid-log phase (i.e., optical density, $OD_{600} = 0.5$) [27]. Afterward, 10 mL seed culture was withdrawn and inoculated into 500-mL flasks with 90 mL fresh medium (i.e., 1:10, v/v inoculation size and working volume = 100 mL), which was incubated under the same conditions to the seed culture preparation for 7 days. The culture was then harvested by centrifugation at 4,000 rpm for 10 min and washed with sterilized deionized (DI) water for three times. The cell pellet was resuspended in 100 mL sterilized DI water as cell inoculum for making biogrout for biocementation.

The Martian Mojave Simulant was the MRS used in this research to make biocemented columns. This simulant was originally developed by the Jet Propulsion Laboratory (USA) scientists working on the Mars Phoenix mission, and it is still used today to develop future missions, support rover operations, and conduct planetary science research [28]. This simulant has similar chemical compositions to the regolith found on Mars with slight variations and provides a good mineralogic analog for the igneous rocks of Mars and their associated weathering products [28]. The Mojave simulant is available commercially for research and education. A noteworthy effort related to Martian concrete was the work by Wan et al. (2016) [29], where the authors proposed a sulfur concrete made with the JSC Mars-1A simulant and the UCS of the sulfur concretes ranged from 1.7 (for a sulfur ratio of 35 wt%) to 60 MPa (for a sulfur ratio of 50 wt%). To the best of our knowledge, there has not been any effort to make concrete with the Mojave Martian simulant nor has there been effort to make biocemented Martian composite except for our previous research [16]. Depending on the particle size, the dry density of the MRS ranges from 911 to 1,384 kg/m^3, the angle of friction ranges from 30 to 31°, and the cohesion ranges from 0.53 to 1.96 kPa. A commercially available version of this simulant, called Mojave Mars Simulant-1 and distributed by the Martian Garden, was purchased for this research. The purchased MRS came as a 10-lb bag with a variety of particle sizes smaller than 1 mm. The MRS was sieved through a series of screens to obtain three groups of MRS with particle sizes of 0.15 ~ 0.25, 0.25 ~ 0.425, and 0.425 ~ 0.85 mm, respectively. All chemical reagents used in this study were ACS grade unless specified otherwise.

2.2. Fabrication of biocemented MRS columns

As depicted in Fig. 1, the biocementation system includes a pump, a biocementation reactor (a clear acrylic cylinder tube with an internal diameter (ID) = 3.8 cm, an outer diameter (OD) = 5.1 cm and height = 12.7 cm), a biogrout sink (a 150-mL beaker below the acrylic cylinder tube), and tubings for biogrout circulation. The MRS columns were

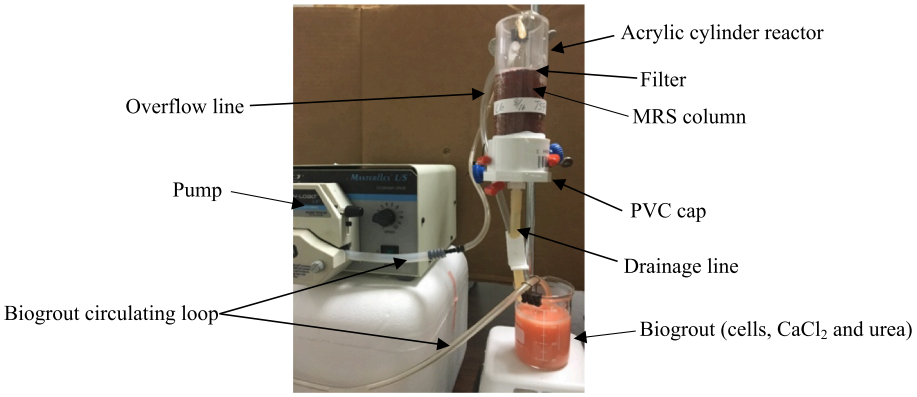

Fig. 1. Biocementation setup (Gleaton et al., 2019).

made in the acrylic tube of which the top was open, and bottom was screwed into a PVC cap. A hole was drilled on the wall of the tube (11.4 cm from the bottom) for directing the biogrout overflow stream back to the beaker below the tube. The PVC cap also had a hole in the center and a barbed hose fitting, and a portion of a tubing was added to the PVC cap to help with the drainage and circulation of biogrout through the acrylic tube. To prevent the loss of MRS particles from the bottom of the acrylic tube, a 40-mesh nylon sheet was placed in between the PVC cap and acrylic tube. On the top of the MRS column, a piece of Scotch-Brite scour pad with a diameter of 3.8 cm was used to help distribute the biogrout evenly on the top of the MRS column while preventing the big particles of $CaCO_3$ precipitate (formed outside the column) from entering and clogging the MRS column. A wax paper (15 cm × 9 cm) was attached along the wall inside the acrylic tube to ease the removal of finished MRS columns from the tube without damaging columns. Prior to biogrouting, 105.0 g of sieved MRS was charged into the acrylic tubes and then rinsed with 150 mL of distilled de-ionized (DDI) water, which was used to facilitate even distribution of biogrout during circulation. Then, the biogrout including *T. striatum* cells, $CaCl_2$, and urea was prepared in a beaker below the acrylic tube and recirculated through the columns from the top of the tube by using a peristaltic pump with a constant pumping rate of 8.0 mL/min. The biogrout circulation was stopped after the designated duration. The columns were drained of any remaining free liquid, removed from the tube, and dried in an oven overnight at 60 °C to stop the microbial activity, quench the biocementation process, and shorten the sample preparation time for analysis, making the biocementation time control more accurate for comparison. Our comparison between oven and natural drying (under room environmental conditions) showed that natural drying resulted in a little better UCS (data not shown) probably because biocementation still occurred during natural drying in the presence of trapped microbial cells, urea, and $CaCl_2$. The dry columns had a dimension of 3.8 cm × 7.6 cm (diameter (D) × height (H)), and their $CaCO_3$ content and UCS were measured.

2.3. Experimental design

A full factorial design with 3 factors, each at 3 levels (i.e., 3^3 design) (Table 1), was used to arrange the experiments for the optimization of UCS of biocemented MRS columns. There were 27 treatments in total, and each treatment was conducted in triplicate. The three factors included MRS particle size, *T. striatum* cell biomass loading, and nutrient (i.e., $CaCl_2$/urea) loading. The three levels of MRS size were 0.15 ~ 0.25, 0.25 ~ 0.425, and 0.425 ~ 0.85 mm. The tested cell biomass loadings included 1.9, 2.9, and 3.8 g/100 mL biogrout. Based upon our previous study [16], the best molar ratio of $CaCl_2$/urea to achieve the optimal UCS of the biocemented MRS column is 1:4.5, which was adopted in this research. Therefore, the three levels of $CaCl_2$ loading were 2, 7.2, and 12.4 g/100 mL biogrout while the corresponding three different urea loadings were 4.9, 17.7, and 30.4 g/100 mL biogrout, i.e., the absolute mass of $CaCl_2$ and urea were varied, whereas their molar ratio was kept at a constant of 1:4.5.

Table 1
Experimental factors and levels for UCS optimization of MRS columns.

Factors	MRS particle size (mm)	Daily cell biomass loading (3 h/21 h, g/day)	Daily nutrient ($CaCl_2$/urea, g/g) loading (g/day)
Levels	0.425 ~ 0.85	0.48/0.48	1.0/2.45
	0.25 ~ 0.425	0.73/0.73	3.6/8.82
	0.15 ~ 0.25	0.95/0.95	6.2/15.2

The biogrout circulation was done by following the standard two-stage operation procedure, which was developed in our previous research [16] (Fig. 2). Briefly, the biogrouting process started with the 1st stage, where only half of the daily cell biomass loading (0.48, 0.73, or 0.95 g cells) was circulated for 3 h to establish cultures inside the MRS column. This was expected to promote the $CaCO_3$ precipitation in the presence of $CaCl_2$/urea. Afterward, in the 2nd stage, the other half of the daily cell biomass loading (i.e., 0.48, 0.73, or 0.95 g cells) was mixed with the daily $CaCl_2$/urea (1 g/2.45 g, 3.6 g/8.82 g, or 6.2 g/15.2 g) to make the biogrout, which was then circulated through the MRS column for 21 h. Such a two-stage biogrouting process was repeated for 2 days continuously. After the biogrouting was finished, the biocemented MRS columns were removed from the reactors and underwent the post-biocementation treatment (described in Section 2.2) prior to the UCS and $CaCO_3$ content analyses.

2.4. Analytical methods

The produced MRS columns with a diameter-to-height ratio of 1:2 (i.e., 3.8:7.6, cm/cm) were subjected to UCS measurement. Since no standard method was developed for UCS measurement of biocemented concrete, the existing standard ASTM C39 [30] was slightly modified to accommodate low UCS of biocemented columns. With the standard loading rate corresponding to a stress rate of 0.25 ± 0.05 MPa/s on the columns, the biocemented MRS columns were usually crushed in a few seconds because of their lower mechanical strength than the conventional concrete. As such, a deformation-driven scheme was used to apply the axial compressive load at a constant rate of 1.0 mm/min [31] for testing the UCS of biocemented MRS columns. With this modified loading rate, a strain rate of about 1.3 %/min was produced, which allowed for the columns to break within 2 min. After the UCS tests, the broken columns were manually separated into three sections (top, middle, and bottom) of the columns, and each section was subject to the analysis of $CaCO_3$ content (%, w/w) via titration method to determine the $CaCO_3$ deposit within different sections of the columns [32]. The correlation between UCS and $CaCO_3$ content of the biocemented MRS columns were studied.

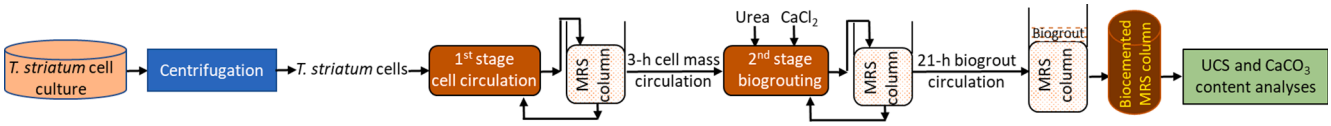

Fig. 2. Standard biogrouting process [16].

2.5. Data analysis

Statistical significance was determined by analysis of variance (ANOVA, $\alpha = 0.05$) using JMP Pro 12 (SAS Institute, Cary, NC, USA) with $p_{critical} = 0.05$. All experiments were conducted in three biological replicates in this study unless specified, otherwise. RSM was utilized to determine the optimum conditions to maximize UCS of the biocemented MRS columns among the conditions stated in Section 2.3. After collecting the data from the UCS measurements, the data were inputted into JMP Pro 12. The response surface design had three factors (regolith particle size, cell biomass loading, and nutrient loading) and one response (UCS). Although urea is one of the critical nutrients, it was not utilized as a factor in RSM optimization because it was collinear with $CaCl_2$ to avoid collinearity of model regression. Therefore, determining the optimum amount of $CaCl_2$ will be enough to ascertain the required urea loading. Carbonate content was not optimized as a response since the goal of MICP process optimization was to maximize the overall UCS of the biocemented MRS columns. By using JMP Pro, the data were modeled, and the prediction formulas were collected. Utilizing the prediction profiler within the modeled data allowed for the determination of the maximum desirability of the data. Lastly, the prediction formulas were utilized to generate surface contour graphs. This process was repeated for each of the regolith particle size ranges (lower, medium, and upper). A quadratic regression model (Eq. (1)) was developed to investigate the effects of all factors, including cell biomass loading, $CaCl_2$ loading, particle size, and their interactions on UCS. Since the quadratic regression model fitted the data better than the linear model, only the quadratic model is reported. After all terms were fitted to the data, a stepwise regression was used to develop a simple and reduced regression model with the highest correlation with the response.

$$UCS = \beta_0 + \sum \beta_i X_i + \sum \beta_{ij} X_i X_j + \sum \beta_{ii} X_i^2 + \varepsilon \quad (1)$$

where, $i = 1 \sim 4$, $j = 1 \sim 4$, β_0 refers to interception, X_1 refers to cell biomass loading, X_2 refers to $CaCl_2$ loading, and X_3 and X_4 refer to particle size. Since particle size is a category variable, a set of dummy variables (X_3 and X_4) were used to indicate the range of particle size. Upper range of particle size corresponded to $X_3 = X_4 = 0$; medium range of particle size corresponded to $X_3 = 1$ and $X_4 = 0$; and lower range of particle size corresponded to $X_3 = X_4 = 1$.

3. Results and discussion

3.1. Effects of particle size, cell biomass loading, and nutrient loading on calcium carbonate precipitate and unconfined compressive strength

3.1.1. Effect of regolith particle size

Under the same cell biomass and nutrient loadings, medium regolith particle size (0.25 ~ 0.425 mm) achieved the highest UCS, such as Sets (1, 10, and 19), (5, 14, and 23), and (9, 18, and 27) (Table 2 and Fig. S1). For example, medium particle size of 0.25 ~ 0.425 mm resulted in the maximum UCS of 388.83 kPa at the same cell biomass loading (2.9 g/100 mL) and nutrient loading (7.2/17.65, g/100 mL) (Fig. S1b). This result is different from the previous results reported by other researchers [11,17,18], where it was reported that the UCS of sand columns increased with the increase of particle size. This discrepancy could be due to the difference in biocementing organism, granular material, cell biomass loading, nutrient loading, and/or other operating conditions. The other reason could be that most previous research only studied two

Table 2
UCS and carbonate content of biocemented MRS columns under different conditions.

Experiment set	Regolith particle size (mm)	Cell biomass loading (g/100 mL)	Nutrient loading ($CaCl_2$/Urea) (g/100 mL)	UCS (kPa)	$CaCO_3$ content (%)
1	0.425 ~ 0.85	1.9	2/4.90	0.00 ± 0.00	11.71 ± 0.55
2	0.425 ~ 0.85	1.9	7.2/17.65	244.13 ± 35.51	11.73 ± 0.75
3	0.425 ~ 0.85	1.9	12.4/30.40	402.03 ± 131.29	15.21 ± 0.41
4	0.425 ~ 0.85	2.9	2/4.90	0.00 ± 0.00	12.00 ± 0.44
5	0.425 ~ 0.85	2.9	7.2/17.65	314.27 ± 55.27	13.17 ± 0.55
6	0.425 ~ 0.85	2.9	12.4/30.40	203.80 ± 23.05	13.77 ± 0.30
7	0.425 ~ 0.85	3.8	2/4.90	0.00 ± 0.00	13.24 ± 0.73
8	0.425 ~ 0.85	3.8	7.2/17.65	328.20 ± 23.76	14.20 ± 0.33
9	0.425 ~ 0.85	3.8	12.4/30.40	498.03 ± 54.23	15.90 ± 0.37
10	0.25 ~ 0.425	1.9	2/4.90	357.40 ± 19.66	12.31 ± 0.38
11	0.25 ~ 0.425	1.9	7.2/17.65	413.23 ± 108.16	11.89 ± 0.73
12	0.25 ~ 0.425	1.9	12.4/30.40	476.10 ± 71.85	16.10 ± 0.34
13	0.25 ~ 0.425	2.9	2/4.90	462.47 ± 68.40	13.53 ± 1.15
14	0.25 ~ 0.425	2.9	7.2/17.65	388.83 ± 30.19	13.26 ± 0.14
15	0.25 ~ 0.425	2.9	12.4/30.40	400.07 ± 236.29	12.97 ± 0.52
16	0.25 ~ 0.425	3.8	2/4.90	518.97 ± 10.10	10.57 ± 0.75
17	0.25 ~ 0.425	3.8	7.2/17.65	685.60 ± 72.97	12.55 ± 0.30
18	0.25 ~ 0.425	3.8	12.4/30.40	517.53 ± 221.29	15.03 ± 0.19
19	0.15 ~ 0.25	1.9	2/4.90	57.01 ± 0.00	13.44 ± 2.56
20	0.15 ~ 0.25	1.9	7.2/17.65	72.12 ± 20.27	13.69 ± 0.33
21	0.15 ~ 0.25	1.9	12.4/30.40	292.37 ± 218.56	14.34 ± 0.66
22	0.15 ~ 0.25	2.9	2/4.90	0.00 ± 0.00	11.26 ± 1.21
23	0.15 ~ 0.25	2.9	7.2/17.65	152.53 ± 88.73	11.37 ± 0.51
24	0.15 ~ 0.25	2.9	12.4/30.40	425.40 ± 237.86	13.81 ± 0.36
25	0.15 ~ 0.25	3.8	2/4.90	584.70 ± 25.94	14.00 ± 0.20
26	0.15 ~ 0.25	3.8	7.2/17.65	367.90 ± 153.07	14.20 ± 0.63
27	0.15 ~ 0.25	3.8	12.4/30.40	276.30 ± 96.94	13.52 ± 0.67

levels of particle size such as fine and coarse. In addition, our data show the particle size doesn't have an evident correlation trend with $CaCO_3$ precipitate, i.e., high $CaCO_3$ content doesn't necessarily lead to high UCS (Fig. S1a-c), which differs from Yang et al. [11] but is similar to Terzis and Laloui [18] and Mahawish et al. [19]. Sand particle size and morphology could affect cell migration and the amount/distribution/crystal size of $CaCO_3$ precipitate within the sand column. Columns with small sand particles have a low void volume that may prohibit cells from migration [6] and reduce the size and spatial distribution uniformity of $CaCO_3$ precipitate along the column [18] (Fig. S2a). This was also found by our previous research that the top half of the MRS column had higher $CaCO_3$ content than the bottom half [16]. With the increase of sand particle size, the homogeneity in the spatial distribution of $CaCO_3$ crystal became better and the quantity of active bonds bridging neighboring sand particles increased, resulting in high UCS [18] (Fig. S2b). However, when the sand particles exceed a certain size, the $CaCO_3$ precipitates are not sufficient or the amount of active $CaCO_3$ bonds is reduced due to the increased void ratio, thus impairing the connections between sand particles (Fig. S2c). Mahawish et al. [19] found that adding fine sand to coarse sand improved UCS of sand columns because fine sand provided more bridging contacts through $CaCO_3$ precipitate between coarse sand particles. Our medium MRS particle size of 0.25 ~ 0.425 mm could be considered equivalent to this method of mixing fine and coarse sand particles, which led to an optimum UCS. Hence, the $CaCO_3$ content doesn't have a necessary connection with UCS of sand columns, and the particle size of granular materials needs to be well controlled to maximize active bonds for bridging contacts. Further research will be required to determine the phenomena occurring during biocementation, quite possibly utilizing X-ray computed tomography (CT) scans and mathematical modeling to determine the internal structures of the biocemented MRS columns.

3.1.2. Effect of nutrient loading

The effects of nutrient ($CaCl_2$/urea) loading on UCS and $CaCO_3$ content varied with regolith particle size and cell biomass loading (Table 2 and Fig. S3). In 0.425 ~ 0.85 mm (Sets 1–9), increasing nutrient loading resulted in the increase of UCS and $CaCO_3$ precipitate at all three cell biomass loadings (Fig. S3a-c). At constant cell biomass loadings, the increase of nutrients could promote cell growth and ureolysis rate to produce more $CaCO_3$ precipitates that fill in the voids within the MRS columns to form more active bonds between regolith particles. In 0.15 ~ 0.25 mm (Sets 19–27), with the increase of nutrient loading, UCS and $CaCO_3$ precipitate increased at low and medium cell loadings (1.9 and 2.9 g/100 mL), while decreased at high cell loading of 3.8 g/100 mL (Fig. S3d-f). As discussed above, small regolith particles can form dense MRS columns, limit cell migration, and reduce distribution uniformity of $CaCO_3$ precipitate within MRS columns, resulting in a low UCS. Therefore, the ureolysis rate at high cell loading could be so fast that a large amount of $CaCO_3$ precipitate is formed and surrounds cells (i.e., cells become nuclei for $CaCO_3$ crystal formation) and stops further MICP. In addition, high cell loading could also form large $CaCO_3$ crystal particles and prohibit the homogenous distribution of $CaCO_3$ precipitate. Similar results were published by Yang et al. [11] and Rowshanbakht et al. [26] who revealed that reduction of bacterial loading increased the $CaCO_3$ precipitate and UCS of sand columns. However, Okwadha and Li [24] and Soon et al. [25] achieved high UCS by increasing cell loading. Such conflicting conclusions could be caused by the interactions between sand particle size, cell loading, and nutrient loading. Using different types of MICP organisms could be another reason because their threshold values of cell loading to maximize UCS might be different.

In 0.25 ~ 0.425 mm (Sets 10–18), the overall UCS and $CaCO_3$ precipitate of MRS columns increased with the increase of nutrient loading at low cell loading of 0.9 g/100 mL (Fig. S3g). At low cell loading, ureolysis rate can be mild and conducive to the gradual formation and homogenous distribution of small and uniform $CaCO_3$ crystals for better bridging between MRS particles [11,26] (Fig. S2b). At medium cell loading, increasing nutrient loading reduced UCS and $CaCO_3$ precipitate, which could be caused by the inhibition of *T. striatum* by high salinity at high nutrient loading (7.2 and 12.4 g/100 mL $CaCl_2$) (Fig. S3h and S4a). When cell loading was increased to 3.8 g/100 mL, UCS of MRS columns increased from 519 to 685 kPa and decreased to 518 kPa with the increase of nutrient loading from 2 to 7.2 and 12.4 g/100 mL, respectively, while $CaCO_3$ precipitate kept increasing in the entire range of nutrient loading (Fig. S3i and S4b). These findings could be because that ureolysis rate of *T. striatum* is moderate at low and medium nutrient loadings such that $CaCO_3$ precipitate is generated gently and forms substantial small and uniform particles with homogenous distribution and a high quantity of active bonds [11]. However, a continuous increase of nutrient loading to 12.4 g/100 mL led to UCS decrease even though $CaCO_3$ precipitate kept increasing. Therefore, ureolysis of *T. striatum* does not appear to be inhibited, but the possible reason is that high nutrient loading resulted in high ureolysis rate and fast $CaCO_3$ precipitate formation, which is unfavorable to the uniform $CaCO_3$ distribution in the MRS column. In addition, such fast ureolysis can easily produce a large amount of big but ununiform $CaCO_3$ crystals, leading to restriction of cell movement, lack of homogeneous distribution, and/or low bonding efficiency [11,20,23,26].

3.1.3. Effect of cell biomass loading

The effect of cell loading is analyzed based on the same regolith particle size and nutrient loading (Table 2 and Fig. S5). In the upper particle size range of 0.425 ~ 0.85 mm (Sets 1–9), UCS of MRS columns was too low to be detected for all cell loadings at the low nutrient loading, whereas $CaCO_3$ precipitate increased consistently, which could be because the low nutrient is a limiting factor that prevents the production of sufficient active bonds in large voids between large MRS particles (Fig. S5a). When nutrients were increased to medium and high levels, the overall UCS and $CaCO_3$ contents of MRS columns increased with the increase of cell loadings (Fig. S5b, c). These findings could indicate that increased cell loadings generated more $CaCO_3$ precipitate and active bonds for efficient bridging between MRS particles. In the medium range of particles of 0.25 ~ 0.425 mm (Sets 10–18), increased cell loading improved the UCS of MRS columns in general, but $CaCO_3$ precipitate reached maximum at low and medium cell loadings and minimum at high cell loading (Fig. S5d-f and S6a-c). Therefore, high cell loading could yield more active $CaCO_3$ deposits to connect MRS particles even though the total $CaCO_3$ content isn't necessarily high. For particle size of 0.15 ~ 0.25 mm (Sets 19–27), increasing cell loading improved the UCS and $CaCO_3$ precipitate of MRS columns in general at low and medium nutrient loadings, while the maximum UCS occurred at medium cell loading (2.9 g/100 mL) when nutrient loading was high (12.4 g/100 mL), but $CaCO_3$ precipitate decreased consistently (Fig. S5g-i). As discussed above in Section 3.1.1, cell migration within the MRS column made with small regolith particles is restricted [6] while nutrients can still penetrate through the column so that the situation of high cell concentration with low nutrient could happen locally, leading to low UCS and $CaCO_3$ deposit (e.g., Set 27).

3.2. Response surface methodology (RSM) for the optimization of MICP process regarding unconfined compressive strength

According to the abovementioned results and discussion in Section 3.1, the three factors (regolith particle size, cell biomass loading, and nutrient loading) and their interactions have significant effects on UCS of the MRS columns. Utilizing the results from Table 2, the data were plugged into a statistical analysis program (JMP Pro) to conduct RSM statistical analysis to determine the optimum conditions for manufacturing biocemented MRS columns. Since the regolith particle size is a categorical, discrete variable, the optimization of UCS was done separately under each particle size group. To visualize the results of the RSM statistical analysis, factor interaction plots and surface contour graphs (Fig. 3) were produced to show the interactions between cell

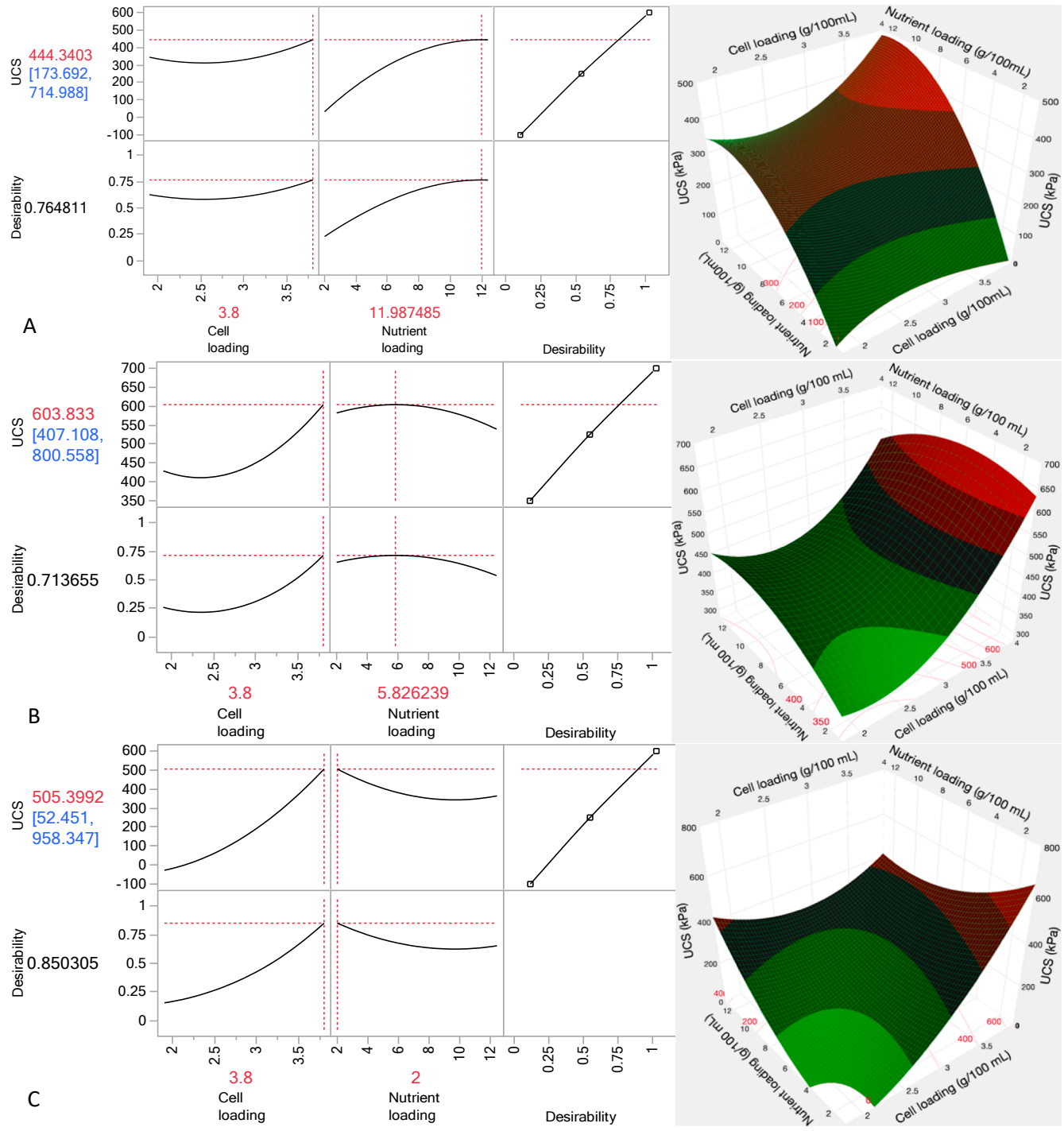

Fig. 3. RSM optimization of UCS under (A) upper particle size; (B) medium particle size; and (C) lower particle size.

biomass and nutrient ($CaCl_2$) loadings and their effects on UCS as well as the optimal combinations of cell biomass and nutrient loadings for maximum UCS with the corresponding desirability. Overall, the medium regolith particle size had the highest optimal UCS, which is 603.83 kPa achieved with the cell loading of 3.8 g/100 mL and nutrient loading of (5.83 $CaCl_2$ + 14.18 urea) g/100 mL (Table 3). In all regolith particle size groups, the higher cell biomass loading pertained to higher UCS, while the optimal nutrient loading increased with the increase of regolith particle size, i.e., bigger particle size needs higher nutrient loading to achieve maximum UCS of the MRS columns. With bigger regolith particle size, the void space between regolith particles is also larger so that more calcium carbonate precipitate is needed to fill the space and

Table 3
RSM statistical analysis for optimizing UCS of the MRS columns.

Regolith particle size (mm)	Cell biomass loading (g/100 mL)	$CaCl_2$/urea (g/100 mL) ($CaCl_2$/urea molar ratio = 1:4.5)	UCS (kPa)	Desirability (%)
0.425 ~ 0.85 (upper)	3.8	11.99/29.17	444.34	76
0.25 ~ 0.425 (medium)	3.8	5.83/14.18	603.83	71
0.15 ~ 0.25 (lower)	3.8	2/4.90	505.40	85

build active bonds bridging regolith particles, thus higher nutrient loading is preferred. In contrast, low nutrient loading is conducive to optimal UCS for small regolith particle size because excessive nutrients could cause overproduction of calcium carbonate precipitate, which may clog the pores among regolith particles and prevent the transport of biogrout and distribution of calcium carbonate precipitate, thus reducing the active bonds and UCS of the MRS columns.

Both linear and quadratic regression models were developed to further investigate the effects of cell biomass loading, nutrient (i.e., $CaCl_2$) loading, regolith particle size, and their interactions on UCS. Since the quadratic regression model fitted the data better than the linear model, only the quadratic model is reported. After all terms were fitted to the data, a stepwise regression was used to develop a simple and reduced regression model with the highest correlation with the response. ANOVA results for the second-order response model are shown in Table 4. ANOVA of the reduced quadratic modeling showed that the fitted model was highly significant with F-value of 151.3 and the corresponding *p*-value of 0.0001 at 95% level of confidence ($p < 0.0001$). Since the computed F-statistic value (151.3) exceeded the F-critical value (2.05), we rejected the null hypothesis (H_0) in favor of the alternative (H_1) based on a type I error rate (the error of rejecting a null hypothesis when it is actually true) of 5%. Therefore, we concluded that a significant relationship exists between UCS and cell biomass loading, $CaCl_2$ loading, particle size, and their interactions. The coefficient of determination of the regression analysis, R^2 value is 0.9724, indicating that approximately 97% of the variability in UCS was explained by the model. As an alternative measure of model adequacy, the adjusted multiple coefficient of determination (adjusted R^2) is 0.9659, indicating that after adjusting the sample size and number of parameters, approximately 96% of the total variation in UCS was explained by the model, which suggests a suitable fitness of the model. The "Lack of Fit F-value" of 1.75 implies that "Lack of Fit" is not significant relative to the pure error and the reduced quadratic model is adequate. RSM developed a reduced quadratic regression model for UCS, as shown in Eq. (2) obtained for the coded factors:

$$UCS = 276.77 + 94.72X_1 + 142.55X_2 - 143.11X_3 - 26.97X_4 + 23.22X_1X_2 + 0.85X_1X_3 + 21.47X_1X_4 + 2.43X_2X_3 + 54.37X_2X_4 + 63.04{X_1}^2 \quad (2)$$

As shown in Table 4, linear effects of cell biomass loading (X_1), nutrient loading (X_2), and particle size (X_3 and X_4) as well as quadratic effects of cell biomass loading (${X_1}^2$) significantly affected UCS ($p < 0.05$). The $CaCl_2$ loading term (X_2) had the most significant effect on UCS, followed by particle size and cell biomass loading based on the F-values. According to F values and *p* values, all interaction terms of cell biomass loading, $CaCl_2$ loading, and particle size had significant effects on UCS. The variance inflation factor (VIF) of all terms except the category variable is 1.0, indicating that there is no multicollinearity for all terms in the reduced quadratic model (Table 5). This model is reliable based on robust orthogonality in the design. However, it must be noted that the statistical models are precise only in specific conditions, e.g., they may be applicable only to the specific microorganism that was used in this study.

4. Conclusions

T. striatum is a new biocementation microorganism and is capable of creating MICP. It was successfully used to manufacture biocemented MRS columns in this study. Three factors, including cell biomass loading, nutrient (i.e., $CaCl_2$/urea) loading, and regolith particle size, were investigated and found to significantly affect the UCS and $CaCO_3$ precipitate of MRS columns. RSM was utilized to optimize these factors to maximize the UCS of MRS columns. The overall UCS of the columns increased with the increase of cell biomass loading, while the medium-sized MRS resulted in the strongest biocemented columns. The effect of $CaCl_2$/urea loading on UCS of MRS columns did not show a consistent trend. Therefore, it can't be determined whether the $CaCl_2$/urea loading has a positive effect on the UCS of the columns or not. The optimum conditions to achieve maximum UCS of the biocemented MRS columns varied with regolith particle size. The maximum UCS of 603.83 kPa was achieved at 0.25 ~ 0.425 mm particle size, 3.8 g/100 mL cell biomass loading, and 5.83/14.18 ($CaCl_2$/urea) g/100 mL nutrient loading. Further research will need to be conducted to determine how the internal structure of MRS columns and the distribution of $CaCO_3$ precipitate within the columns affect the overall strength of columns.

Table 4
ANOVA for reduced quadratic model.

Source	Sum of squares	df	Mean square	F-value	P-value
Model	2.1×10^6	10	2.1×10^5	151.3	<0.0001
X_1-Cell biomass loading	3.2×10^5	1	3.2×10^5	232.3	<0.0001
X_2-nutrient ($CaCl_2$/urea) loading	7.3×10^5	1	7.3×10^5	526.2	<0.0001
X_3-Particle size	9.0×10^5	2	4.5×10^5	324.6	<0.0001
X_1X_2	12936.3	1	12936.3	9.3	0.0039
X_1X_3	11514.8	2	5757.4	4.1	0.0226
X_2X_3	74254.7	2	37127.3	26.7	<0.0001
${X_1}^2$	47693.1	1	47693.1	34.3	<0.0001
Residual	59770.8	43	1390.0	NA	NA
Lack of Fit	30446.4	16	1902.9	1.75	0.0964
Pure Error	29324.3	27	1086.0	NA	NA
Corrected Total	2.2×10^6	53			
$R^2 = 0.9724$, and adjusted $R^2 = 0.9659$					

Table 5
Regression coefficients and their VIF in reduced quadratic model.

Term	Coefficient estimate	df	Standard error	Variance inflation factor
Intercept	276.77	1	8.79	NA
X_1-Cell biomass loading	94.72	1	6.21	1.0
X_2-nutrient ($CaCl_2$/urea) loading	142.55	1	6.21	1.0
X_3	−143.11	1	7.18	NA
X_4	−26.97	1	7.18	NA
X_1X_2	23.22	1	7.61	1.0
X_1X_3	0.85	1	8.79	NA
X_1X_4	21.47	1	8.79	NA
X_2X_3	2.43	1	8.79	NA
X_2X_4	54.37	1	8.79	NA
${X_1}^2$	63.04	1	10.76	1.0

CRediT authorship contribution statement

Jason Gleaton: Investigation, Writing – original draft, Formal analysis. **Zhengshou Lai:** Investigation, Formal analysis. **Rui Xiao:** Data curation, Investigation. **Ke Zhang:** Data curation, Writing – review & editing. **Qiushi Chen:** Funding acquisition, Supervision, Writing – review & editing. **Yi Zheng:** Funding acquisition, Supervision, Conceptualization, Methodology, Writing – review & editing, Project administration.

Declaration of Competing Interest

The authors declare that they have no known competing financial interests or personal relationships that could have appeared to influence the work reported in this paper.

Acknowledgements

This work was supported by the National Aeronautics and Space

Administration (NASA) of the United States through South Carolina Space Consortium Grants [Grant numbers NNX15AK53A and NNX15AL49H, 2016, 2017].

Appendix A. Supplementary data

Supplementary data to this article can be found online at https://doi.org/10.1016/j.conbuildmat.2021.125741.

References

[1] D. Ariyanti, N.A. Handayani, H. Hadiyanto, An overview of biocement production from microalgae, Internat J. Sci. Eng. Dessy Ariyanti Al. 2 (2011) 30–33, https://doi.org/10.12777/ijse.2.2.31-33.

[2] D. Ariyanti, N.A. Handayani, H. Hadiyanto, Feasibility of using microalgae for biocement production through, Bioprocess. Biotech. 2 (2012) 8–11, https://doi.org/10.4172/2155-9821.1000111.

[3] V. Achal, A. Mukherjee, A review of microbial precipitation for sustainable construction, Constr. Build. Mater. 93 (2015) 1224–1235, https://doi.org/10.1016/j.conbuildmat.2015.04.051.

[4] D. Mujah, M.A. Shahin, L. Cheng, State-of-the-art review of biocementation by microbially induced calcite precipitation (MICP) for soil stabilization, Geomicrobiol. J. 34 (6) (2017) 524–537, https://doi.org/10.1080/01490451.2016.1225866.

[5] M.J. Castro-Alonso, L.E. Montanez, M.A. Sanchez-Munoz, M.R.M. Franco, R. Narayanasamy, N. Balagurusamy, Microbially induced calcium carbonate precipitation (MICP) and its potential in bioconcrete: Microbiological and molecular concepts, Front. Mater. 6 (2019) 126, https://doi.org/10.3389/fmats.2019.00126.

[6] M. Umar, K.A. Kassim, K.T. Ping Chiet, Biological process of soil improvement in civil engineering: A review, J. Rock Mech. Geotech. Eng. 8 (5) (2016) 767–774, https://doi.org/10.1016/j.jrmge.2016.02.004.

[7] P. Anbu, C.-H. Kang, Y.-J. Shin, J.-S. So, Formations of calcium carbonate minerals by bacteria and its multiple applications, Springerplus 5 (2016) 250, https://doi.org/10.1186/s40064-016-1869-2.

[8] N.K. Dhami, M.S. Reddy, M.S. Mukherjee, Biomineralization of calcium carbonates and their engineered applications: A review, Front. Microbiol. 4 (2013) 1–13, https://doi.org/10.3389/fmicb.2013.00314.

[9] V. Stabnikov, V. Ivanov, A. Vaseashta, Biotechnological immobilization of chemical, biological, and radioactive pollutants on land and infrastructure demolition waste after industrial accident, military action, or terrorist attack, in: F. Pacheco-Torgal, V. Ivanov, D.C.W. Tsang (Eds.), Woodhead Publishing Series in Civil and Structural Engineering, Bio-based materials and biotechnologies for eco-efficient construction. Elsevier, Cambridge, MA, United States, 2020, pp. 377-393. doi.org/10.1016/B978-0-12-819481-2.00018-0.

[10] V. Ivanov, J. Chu, Applications of microorganisms to geotechnical engineering for bioclogging and biocementation of soil in situ, Rev. Environ. Sci. Biotechnol. 7 (2008) 139–153, https://doi.org/10.1007/s11157-007-9126-3.

[11] D. Yang, G. Xu, Y. Duan, Effect of particle size on mechanical property of bio-treated sand foundation, Appl. Sci. 10 (2020) 8294, https://doi.org/10.3390/app10228294.

[12] A.M. Sharaky, N.S. Mohamed, M.E. Elmashad, N.M. Shredah, Application of microbial biocementation to improve the physico-mechanical properties of sandy soil, Constr. Build. Mater. 190 (2018) 861–869, https://doi.org/10.1016/j.conbuildmat.2018.09.159.

[13] S. Joshi, S. Goyal, M.S. Reddy, Influence of nutrient components of media on structural properties of concrete during biocementation, Constr. Build. Mater. 158 (2018) 601–613, https://doi.org/10.1016/j.conbuildmat.2017.10.055.

[14] G. Kaur, N.K. Dhami, S. Goyal, A. Mukherjee, M.S. Reddy, Utilization of carbon dioxide as an alternative to urea in biocementation, Constr. Build. Mater. 123 (2016) 527–533, https://doi.org/10.1016/j.conbuildmat.2016.07.036.

[15] J.T. DeJong, B.M. Mortensen, B.C. Martinez, D.C. Nelson, Bio-mediated soil improvement, Ecol. Eng. 36 (2010) 197–210.

[16] J. Gleaton, Z. Lai, R. Xiao, Q. Chen, Y.i. Zheng, Microalga-induced biocementation of martian regolith simulant: Effects of biogrouting methods and calcium sources, Constr. Build. Mater. 229 (2019) 116885, https://doi.org/10.1016/j.conbuildmat.2019.116885.

[17] T. Hoang, J. Alleman, B. Cetin, M. Cetin, S.-G. Choi, Engineering properties of biocementation coarse-and fine-grained sand catalyzed by bacterial cells and bacterial enzyme, J. Mater. Civil Eng. 32 (2020), https://doi.org/10.1061/(ASCE)MT.1943-5533.0003083.

[18] D. Terzis, L. Laloui, 3-D micro-architecture and mechanical response of soil cemented via microbial-induced calcite precipitation, Sci. Rep. 8 (2018) 1416, https://doi.org/10.1038/s41598-018-19895-w.

[19] A. Mahawish, A. Bouazza, W.P. Gates, Effect of particle size distribution on the bio-cementation of coarse aggregates, Acta Geotech. 13 (4) (2018) 1019–1025, https://doi.org/10.1007/s11440-017-0604-7.

[20] W. De Muynck, K. Verbeken, N. De Belie, W. Verstraete, Influence of urea and calcium dosage on the effectiveness of bacterially induced carbonate precipitation on limestone, Ecol. Eng. 36 (2) (2010) 99–111, https://doi.org/10.1016/j.ecoleng.2009.03.025.

[21] W. De Muynck, N. De Belie, W. Verstraete, Microbial carbonate precipitation in construction materials: A review, Ecol. Eng. 36 (2) (2010) 118–136, https://doi.org/10.1016/j.ecoleng.2009.02.006.

[22] N.W. Soon, L.M. Lee, T.C. Khun, H.S. Ling, Improvements in engineering properties of soils through microbial-induced calcite precipitation, KSCE J. Civ. Eng. 17 (4) (2013) 718–728, https://doi.org/10.1007/s12205-013-0149-8.

[23] B.M. Mortensen, M.J. Haber, J.T. Dejong, L.F. Caslake, D.C. Nelson, Effects of environmental factors on microbial induced calcium carbonate precipitation, J. Appl. Microbiol. 111 (2011) 338–349, https://doi.org/10.1111/j.1365-2672.2011.05065.x.

[24] G.D.O. Okwadha, J. Li, Optimum conditions for microbial carbonate precipitation, Chemosphere 81 (9) (2010) 1143–1148, https://doi.org/10.1016/j.chemosphere.2010.09.066.

[25] N.W. Soon, L.M. Lee, T.C. Khun, H.S. Ling, Factors affecting improvement in engineering properties of residual soil through microbial-induced calcite precipitation, J. Geotech. Geoenviron. 140 (2014), https://doi.org/10.1061/(ASCE)GT.1943-5606.0001089.

[26] K. Rowshanbakht, M. Khamehchiyan, R.H. Sajedi, M.R. Nikudel, Effect of injected bacterial suspension volume and relative density on carbonate precipitation resulting from microbial treatment, Ecol. Eng. 89 (2016) 49–55, https://doi.org/10.1016/j.ecoleng.2016.01.010.

[27] R. Xiao, X. Li, E. Leonard, N. Tharayil, Y. Zheng, Investigation on the effects of cultivation conditions, fed-batch operation, and enzymatic hydrolysate of corn stover on the astaxanthin production by *Thraustochytrium striatum*, Algal Res. 39 (2019) 101475, https://doi.org/10.1016/j.algal.2019.101475.

[28] G.H. Peters, W. Abbey, G.H. Bearman, G.S. Mungas, J.A. Smith, R.C. Anderson, S. Douglas, L.W. Beegle, Mojave Mars Simulant-Characterization of a new geologic Mars analog, Icarus 197 (2) (2008) 470–479, https://doi.org/10.1016/j.icarus.2008.05.004.

[29] L. Wan, R. Wendner, G. Cusatis, A novel material for *in situ* construction on Mars: experiments and numerical simulations, Constr. Build. Mater. 120 (2016) 222–231, https://doi.org/10.1016/j.conbuildmat.2016.05.046.

[30] ASTM International, Standard Test Method for Compressive Strength of Cylindrical Concrete Specimens (C39), West Conshohocken, PA: ASTM International, (2016) doi:10.1520/C0039_C0039M-12.

[31] L. Cheng, R. Cord-Ruwisch, M.A. Shahin, Cementation of sand soil by microbially induced calcite precipitation at various degrees of saturation, Can. Geotech. J. 50 (1) (2013) 81–90, https://doi.org/10.1139/cgj-2012-0023.

[32] D.L. Rowell, Soil Science: Methods and Applications. Harlow: Longman Scientific & Technical. (1994).